Hindawi
Science and Technology of Nuclear Installations
Volume 2021, Article ID 7035787, 12 pages
https://doi.org/10.1155/2021/7035787

Research Article

Integrity Evaluation of a Reactor Pressure Vessel Based on a Sequential Abaqus-FRANC3D Simulation Method

M. Annor-Nyarko [1,2,3] **and Hong Xia** [1,2]

[1]*Key Laboratory of Nuclear Safety and Advanced Nuclear Energy Technology, Ministry of Industry and Information Technology, Harbin Engineering University, Harbin 150001, China*
[2]*Fundamental Science on Nuclear Safety and Simulation Technology Laboratory, Harbin Engineering University, Harbin 150001, China*
[3]*Nuclear Installations Directorate, Nuclear Regulatory Authority, Kwabenya, Ghana*

Correspondence should be addressed to Hong Xia; xiahong@hrbeu.edu.cn

Received 16 May 2021; Revised 16 July 2021; Accepted 23 August 2021; Published 7 September 2021

Academic Editor: Massimo Zucchetti

The safety-risk pressurized thermal shock (PTS) have on a reactor pressure vessel (RPV) is one of the most important studies for the lifetime ageing management of a reactor. Several studies have investigated PTS induced by postulated accidents and other anticipated transients. However, there is no study that analyzes the effect of PTS induced by one of the most frequent anticipated operational occurrences—inadvertent operation of the safety injection system. In this paper, a sequential Abaqus-FRANC3D simulation method is proposed to study the integrity status of an ageing pressurized water reactor subjected to PTS induced by inadvertent actuation of the safety injection system. A sequential thermal-mechanical coupling analysis is first performed using a three-dimensional reactor pressure vessel finite element model (3D-FEM). A linear elastic fracture mechanics submodel with a postulated semielliptical surface crack is then created from the 3D-FEM. Subsequently, the submodel is used to evaluate the stress intensity factors based on the M-integral approach coupled within the proposed simulation method. Finally, the stress intensity factors (SIFs) obtained using the proposed method are compared with the conventional extended finite element method approach, and the result shows a good agreement. The maximal thermomechanical stress concentration was observed at the inlet nozzle-inner wall intersection. In addition, The ASME fracture toughness of the reactor vessel's steel compared with SIFs show that the PTS event and crack configuration analysed may not pose a risk to the integrity of the RPV. This work serves as a critical reference for the ageing management and fatigue life prediction of reactor pressure vessels.

1. Introduction

The effect of ageing degradation mechanisms in nuclear power plants (NPPs) may result in a substantial loss of plant availability and costly part replacement [1]. In addition, the re-licensing regime of ageing NPPs is largely premised on the integrity assessment of critical components such as the reactor pressure vessel (RPV). The structural integrity of the RPV is a key safety priority in the operation of ageing pressurized water reactor (PWR) NPPs since it technically determines the feasible lifetime of the reactor [2]. Furthermore, under some NPP transient conditions, a small defect of the size of the nondestructive testing limit in an ageing RPV may rapidly grow leading to damage or failure. Therefore, structural integrity analysis of vital components such as RPV subjected to potential transient loading from anticipated operational occurrences (AOOs) or postulated accidents (PAs) is essential to guarantee the safety of the whole NPP. In addition, integrity assessment results inform operators about the development of predictive maintenance and ageing management strategies that may prevent catastrophic failures of the RPV equipment.

A major risk to ageing RPVs is the exposure to pressurized thermal shock (PTS) induced by temperature and internal pressure loads from emergency cooling water triggered by AOOs or PA events [3]. The PTS initiating

events that may arise during the operation of NPPs are mainly categorized based on their frequency of occurrence in the plant's lifetime. AOO transients, categorized as condition II events, must not escalate to condition III or IV postulated accidents under any NPP incident. Generally, AOO transients such as the inadvertent actuation of the safety injection system (SIS) or make-up systems occur in pressurized water reactors. This event involves the filling of the PWR's pressurizer and subsequent discharge of the water content through water safety or relief valves [4]. The filling of the pressurizer of PWRs may be initiated through an AOO heat-up or water mass addition event. In both events, the reactor coolant surges into the pressurizer, fills it, and departs the RCS through power-operated relief or pressurizer safety valves. The heat-up events usually cause the pressure and water levels of the pressurizer to rise, as the reactor coolant expands, until the reactor is automatically tripped by the sense of a pressurizer high-level signal. In a water mass addition event, such as an inadvertent operation of the emergency core cooling system (ECCS), the inadvertent opening of a pressurizer power-operated relief valve, or a chemical and volume control system (CVCS) malfunction, the tripped reactor will not cause the stoppage of the flow of water from the ECCS into the RCS. The pressurizer level will continue to increase until it reaches the water-solid pressurizer condition or a reactor operator terminates the safety injection flow, following the required plant emergency procedures, before reaching a more severe condition III event [4, 5]. It is worth noting that a condition II small break loss of coolant accident (SBLOCA) that is initiated from an anticipated transient has a higher frequency of occurrence in an NPP than a condition III SBLOCA. Also, Mukin et al. averred from a thermal-hydraulic screening analysis that the inadvertent opening of a pressurizer power-operated relief valve, which is an AOO event, contributes significantly to PTS due to its high chance of occurrence [6]. Therefore, the high frequency of AOO events occurring in the lifetime of a NPP, in comparison with the extensively studied postulated accidents, may have a critical effect on the physical characteristics of the RPV and other essential reactor equipment [4].

Several studies on the integrity assessment of RPV subjected to PTS loadings are mainly on the PTS initiated by postulated accidents [3]. Chen et al. have performed the structural integrity assessment of the RPV under the PTS loading initiated by a loss of coolant accident (LOCA) [7]. Also, Jhung et al. have evaluated the structural integrity of RPV based on pressurized thermal shock caused by SBLOCA [8]. Murtaza and Hyder have investigated the fracture mechanics analysis of the set-in nozzle of a RPV based on SBLOCA and Rancho-Seco transient events [9]. Zhu et al. have evaluated the fatigue failure of turbine bladed disks under cyclic loadings using a probabilistic modeling approach [10, 11]. Similarly, He and Isozaki have performed an integrity assessment of the RPV of Qinshan NPP under SBLOCA, LBLOCA, and Rancho-Seco PTS transient events [12]. However, the evaluation of the structural integrity of an ageing RPV subjected to PTS from anticipated transients is scarcely studied, despite its relatively high frequency [4, 13, 14]. Furthermore, nuclear safety requirements obligate operators to investigate all potential AOO- and PA-induced PTS events. This forms part of the overall integrity assessment and justification of ageing NPP RPV safety margins in license extension applications [15].

Additionally, the repeated injection of emergency coolant in the SIS inadvertent operation induces thermal stresses in regions of the PWR RPV in contact with the cooling water [16]. These thermal stresses coupled with high internal pressure can cause preexisting defects in the RPV material to increase, leading to damage, leakage, or the possibility of failure [17, 18]. Therefore, a complete safety assessment of ageing NPP must include the integrity analysis of RPV subjected to PTS loads from both anticipated transients and postulated accidents. This is critical for decisions on continuous operation, ageing management, shutdown, or service life extension for ageing NPPs.

Consequently, this study presents a sequential Abaqus-FRANC3D FE method for the evaluation of the structural integrity of an ageing double-circuit PWR reactor pressure vessel subjected to PTS loadings caused by the inadvertent operation of a safety injection system. A sequential thermal-mechanical coupling analysis is first performed to determine the highest stress location in a 3D-FE RPV model developed in Abaqus. A numerical submodeling technique is then applied to evaluate the stress intensity factors (K_I) of an assumed semielliptical surface crack set at the highest stress location in the RPV submodel. Subsequently, K_I values at the deepest crack point are evaluated using the M-integral approach and extended finite element method (XFEM). Finally, K_I is compared with ASME fracture toughness of the RPV steel (K_{IC}) to determine the safety risk the inadvertent operation of the SIS poses on the RPV. The novelties in this work are summarized as follows:

(1) The work proposes a sequential Abaqus-FRANC3D simulation method to investigate the integrity risk posed by the most frequent anticipated operational occurrence (inadvertent operation of SIS) on an ageing RPV. This approach reduces the computational cost in the FE estimation of stress intensity factors in an integrity evaluation of complex geometries.

(2) The integrity parameter, K_I, calculated using the M-integral approach coupled within the proposed method is in agreement with the conventional XFEM approach, confirming its accuracy.

(3) This investigation serves as a preliminary framework for evaluating the effect of other anticipated operating transients on the integrity of an ageing RPV.

2. Background

2.1. System Analysis and Reference Transient. The SIS is a critical safety feature in a nuclear power plant that injects cold water into the RCS during loss of coolant accidents (LOCA). A typical SIS of a double-circuit PWR has four high-pressure safety injection (HPSI) pumps. The inlets of

two of the pumps are connected to the refueling water storage tank (RWST) via power operation isolation and check valves. Also, all inlets of the two pumps are connected to the outlets of the shutdown margin pumps via power operation isolation valves. The outlets of the pumps are connected to a common pipe header with four discharge pipelines connected to the hot legs or cold legs of the RCS. Under the condition of the safety injection, the HPSI pumps enable cold water from the RWST to be pumped into the reactor core [19]. Events leading to the inadvertent injection of colder water directly into the downcomer result in the increase of the core power and pressurizer level. Also, the frequent occurrence of inadvertent operation of SIS during the lifetime of PWRs either by a control system malfunction or by an operator error may cause thermal stresses in the inlet nozzle and inner surface of the RPV wall [4].

2.2. RPV Material Properties. The RPV material is made of ferritic low alloy SA508 Class 3 steel. The material is characterized as homogenous, isotropic, elastic, and temperature-dependent. The RPV thermomechanical properties (thermal conductivity λ, mean thermal expansion coefficient α, elastic modulus E, and specific heat capacity C) are listed in Table 1 [12]. The mean linear thermal expansion coefficients used for the thermomechanical stress calculations were converted to the stress-free reference temperature of 289°C following the conversion approach described in [20]. In addition, the yield strength of vessel material at room temperature, its density, and its Poisson's ratio are 450 MPa, 7600 kgm^{-3}, and 0.3, respectively, as reported in [12, 21]. Figure 1 represents the stress-strain characteristics of the RPV material obtained from experimental tensile tests performed at room and high temperatures [9]. Also, the Ramberg–Osgood power law expressed in equation (1) depicts the nonlinear behavior of the vessel material:

$$\frac{\varepsilon E}{\sigma_0} = \frac{\sigma}{\sigma_0} + \alpha\left(\frac{\sigma}{\sigma_0}\right)^n, \tag{1}$$

where $\varepsilon, E, \sigma_0, n$, and α, respectively, denote the total strain, Young's modulus, yield strength, hardening exponent, and material constant.

2.3. ASME RPV Material Fracture Toughness. The high-energy neutron from the reactor core causes a decrease in the RPV material's fracture toughness and an upward shift in the nil-ductility transition temperature. In this study, the fracture behavior of the referenced RPV material ($\mathrm{K_{IC}}$) is estimated using the main steel parameters in Table 1 and ASME empirical formula expressed as

$$\mathrm{K_{IC}} = 36.5 + 22.783\exp\left[0.036\left(\mathrm{T} - \mathrm{RT_{NDT}}\right)\right], \tag{2}$$

where T and $\mathrm{RT_{NDT}}$ are material temperature and nil-ductility transition temperature, respectively [22–24]. The temperature, $\mathrm{RT_{NDT}}$, is given as follows:

$$\mathrm{RT_{NDT}} = \mathrm{RT_{NDT(}}_{i)} + \Delta\mathrm{RT_{NDT}} + \mathrm{M}, \tag{3}$$

where

$$\Delta\mathrm{RT_{NDT}} = (\mathrm{CF})f^{(0.28-0.10\ \log\ f)}, \tag{4}$$

$$f = f_s \exp\left(-0.00945a\right), \tag{5}$$

$$M = 2\sqrt{\sigma_i^2 + \sigma_\Delta^2}, \tag{6}$$

$$\mathrm{CF} = \sum_{i=1}^{n}\left[A_i \times f_i^{\left(0.28-0.10f_i\right)}\right] \times \left(\sum_{i=1}^{n}\left[f_i^{\left(0.28-0.10f_i\right)}\right]\right)^{-1}, \tag{7}$$

where $\mathrm{RT_{NDT(}}_{i)}$, M, $\Delta\mathrm{RT_{NDT}}$, f, and CF are the reference temperature of un-irradiated RPV material, average safety margin, mean transition temperature shift, neutron irradiation fluence (10^{19}°n/cm^2), and chemistry factor of RPV material, respectively. Also, n, A_i, and f_i are the radiation monitoring points, measured values for $\mathrm{RT_{NDT(}}_{i)}$, and fast neutron fluence per irradiation monitoring point, respectively. σ_Δ and σ_I represent the standard deviation for $\Delta\mathrm{RT_{NDT}}$ and $\mathrm{RT_{NDT(}}_{i)}$, fs is the neutron fluence at the inner surface of the vessel, and a (mm) is the crack depth. It is conservatively assumed that the inner surface and inlet nozzle of the RPV will be subjected to a neutron fluence of 4×10^{19} n/cm^2 at the end of life of the referenced double-circuit PWR. Also, the main random variables of the RPV steel used in this study, shown in Table 2, were derived using the prediction function [25].

From equations (2)–(6) and assumed random variables in Table 2, $\mathrm{RT_{NDT}}$ at 1/4 vessel wall thickness is calculated as

$$\mathrm{RT_{NDT}} = -20 + 52.6 \times 1.4 + 2\sqrt{(9.0)^2 + (9.4)^2} = 79.7\ ^\circ\mathrm{C}. \tag{8}$$

Equation (2) can be expressed as

$$\mathrm{K_{ICv}} = 36.5 + 22.783\ \exp\left[0.036\left(T - 79.7\right)\right]. \tag{9}$$

In addition, the fracture toughness expression for the inlet nozzle-vessel wall intersection steel, based on the ASME code IWB-3613, is given as

$$\mathrm{K_{ICn}} = 25.81 + 16.11\ \exp\left[0.036\left(T - 79.7\right)\right]. \tag{10}$$

The upper bound limiting criteria for the fracture toughness curve (equations (9) and (10)) were estimated, based on the API 579-1/ASME FFS-1 standard, as $\mathrm{K_{ICv}} = 220\ \mathrm{MPa}\sqrt{\mathrm{m}}$ and $\mathrm{K_{ICn}} = 155.6\ \mathrm{MPa}\sqrt{\mathrm{m}}$, respectively. Figure 2 show the fracture toughness behaviour of the RPV steel material.

3. Method

3.1. Reference Transient Event and Sequential Analysis Implementation. The AOO PTS event initiated by an inadvertent SIS operation selected for this study was investigated by Wang et al. [19]. This type of event frequently occurred in the lifetime of PWR NPPs as reported in IAEA operational experience feedback reports [14, 26]. The unexpected action of the SIS caused the injection of cold water

Table 1: Thermomechanical properties of the RPV material.

T (°C)	λ (W/m °C)	E (GPa)	α (10^{-6} 1/°C)	C (10^6 J/m^3°C)
50	38.3	191	13.8	465.8
100	38.8	187	14.2	489.0
150	38.8	184	14.7	508.4
200	38.6	181	15.5	527.7
250	38.1	178	17.5	545.8
300	37.5	174	18.6	567.7
350	36.8	171	18.6	588.4

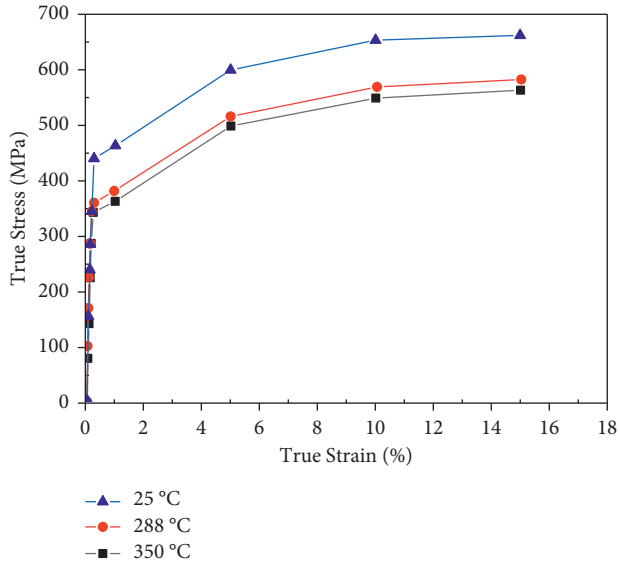

Figure 1: True stress-strain characteristics of the RPV's steel at different temperatures.

Table 2: Main random parameters of SA508 Class 3 steel.

Parameter	Average	Standard deviation	Distribution type
Crack depth (m)	0.042	1.0	Exponential
Phosphorus content (wt. %)	0.008	0.001	Normal
Copper content (wt. %)	0.07	0.01	Normal
Nickel content (wt. %)	0.76	0.05	Normal
$RT_{NDT(i)}$ (°C)	−20	9.0	Normal
f_s (10^{19} n/cm^2)	1.0 ~ 7.0	10% of mean value	Normal
ART_{NDT} (°C)	RG.166 Rev.2	9.4	Normal
$K_{IC\ max} = 220$ (MPa.m$^{1/2}$)	ORNL method		Weibull

into the RCS leading to a rise in the loop pressure. The maximum injection flow rate was approximately 13 kg/s. The cooling water temperature and internal pressure distributions obtained from the AOO event are shown in Figure 3. Also, the critical phase during the transient event was observed at the pressure value of 14.7 MPa at 642 s. The initial temperatures of the inner and outer surface of the RPV model are conservatively set to 289°C and 20°C, respectively. In addition, the heat transfer coefficient between the air and the outer surface vessel is assumed to be 20 W/m^2°C. The structural integrity evaluation was done following the sequential simulation process shown in Figure 4.

3.2. Heat Transfer Coefficient Estimation. To evaluate the heat transferred from the injected cold water to the inner parts of the RPV model, an approximate heat transfer coefficient (h) was estimated using the following equation [27, 28]:

$$h = \frac{N_u k}{D}, \tag{11}$$

where N_u, h, D, and k is the Nusselt number, heat transfer coefficient, hydraulic diameter (the diameter of the hot leg, 0.699 m, of the referenced PWR is assumed in the present FE model), and thermal conductivity of water, respectively. The Nusselt number is expressed as

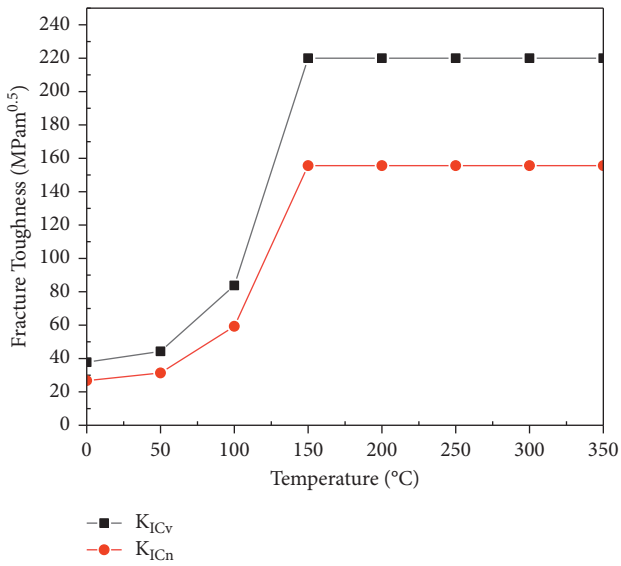

Figure 2: Fracture toughness curve of the irradiated referenced RPV steel.

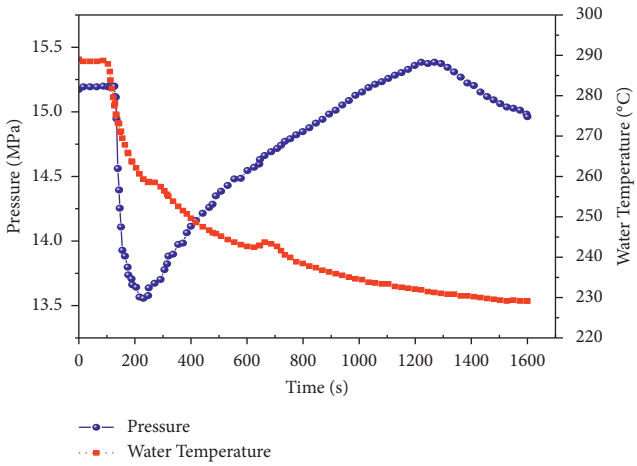

Figure 3: AOO transient reference data for temperature and pressure histories.

$$N_u = C(\mathrm{GrPr})^n. \tag{12}$$

However, the Grashof and Prandtl numbers are determined from [27]

$$\mathrm{Gr} = \frac{D^3\rho^2 g\beta\Delta T}{\mu^2}, \tag{13}$$

$$\mathrm{Pr} = \frac{C_p\mu}{k}, \tag{14}$$

where β, C_p, $g, \Delta T$, ρ, and μ are the isobaric cubic expansion coefficient, specific heat capacity, gravity, temperature change, density, and viscosity, respectively [29, 30]. The heat transfer coefficient was then derived as follows:

$$h = Ck\left(\frac{D^2\rho^2 g\beta\Delta T}{\mu^2}\mathrm{Pr}\right)^n. \tag{15}$$

$C = 0.590$, $n = 0.3$, and $k = 0.6096$ W/m K are assumed in computing the heat transfer coefficient. Also, the physical properties of the coolant water; β, C_p, g, ρ, and μ are estimated at a PWR operational pressure of 14.7 MPa and $\Delta T = 289^\circ$C using STEAMEST software tool developed by [29].

3.3. Reactor Pressure Vessel Model. The core beltline and connecting nozzle area are considered as part of the key regions of the RPV due to the exposure to high neutron irradiation that leads to an increase in nil-ductility transition temperature and embrittlement [31]. Therefore, the three-dimensional (3D) design of one-half of a double-circuit PWR RPV, without cladding, capturing a section of the beltline and inlet nozzle areas shown in Figure 5 was adopted in this study. The inner diameter of the RPV, vessel wall thickness, and nozzle's inner diameter are 3.374 m, 0.170 m, and 0.70 m, respectively.

3.4. Thermal and Thermomechanical Models. The RPV FE models used for the sequential thermal-mechanical coupling analysis were preprocessed and meshed using the finely discretized hexahedral element type in HyperMesh software [32]. The thermal and thermomechanical FE models were meshed using element types DC3D20 and C3D20R, respectively, as shown in Figure 6(a). The bottom section of the FE model is constrained to limit the displacement of the rigid body, but the upper section is left in free state. Symmetricity boundary conditions are also applied. The heat transfer coefficient between the ambient air and the outer surface of the RPV was taken to be 20 W/m$^{2\circ}$C and outer vessel temperature as 20°C. The temperature and pressure histories obtained from the reference anticipated transient event, in Figure 5, and a heat expansion coefficient of 8450 w/m$^{2\circ}$C conservatively estimated from equation (15) were assumed as loads and input for the sequential coupling analysis. The loads and boundary conditions depicted in the RPV global model shown in Figure 6(b) were used to simulate the thermomechanical stresses in Abaqus software.

3.5. Fracture Mechanics Submodel. The majority of failures associated with the RPV have been traced to shallow cracks. Axial surface cracks are also known to be more critical than circumferential surface cracks due to the maximum stress they experience in a vessel configuration [33]. Furthermore, probabilistic fracture mechanics studies reported in many literature studies show that shallow cracks contribute more to the probability of crack initiation in RPV than deep cracks [10]. This is because thermomechanical loading and neutron irradiation are more severe at the surface of the RPV [16]. In this study, an axially oriented semielliptical surface crack is assumed. Also, the crack geometry applied as shown in Figure 7(a) had a depth (a) of one-fourth the RPV wall thickness with an aspect ratio of $(2c/a) = 6$ [34]. These

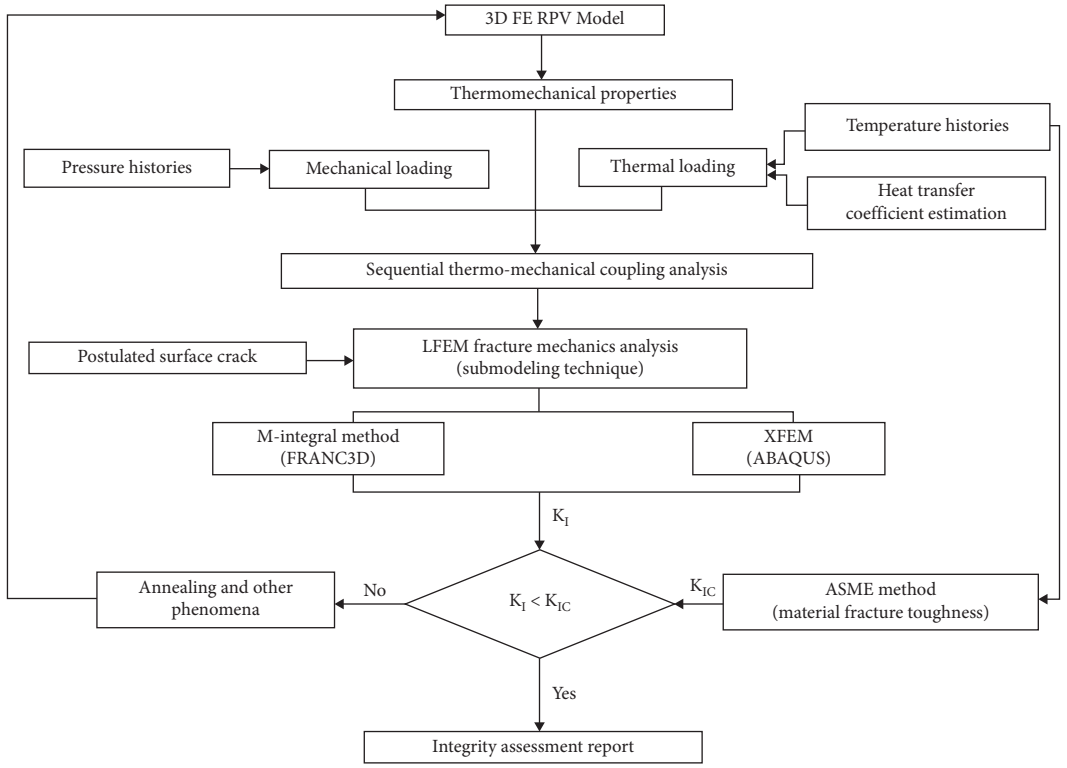

Figure 4: Flow chart of the structural integrity assessment of RPV subjected to AOO PTS loads.

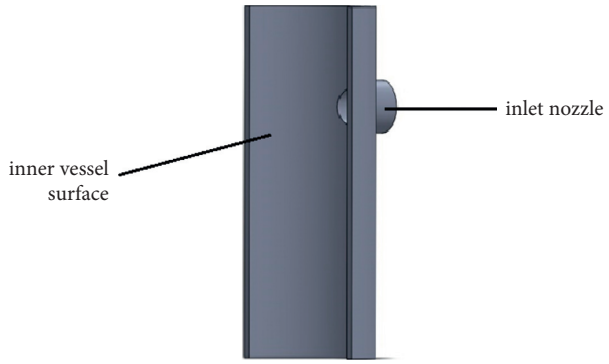

Figure 5: Geometry of the RPV with an inlet nozzle.

postulated crack size and aspect ratio are mostly observed during nondestructive testing or expected during the lifetime of the NPP [35].

The node-based submodels shown in Figures 8 and 9 which comprise the highest stress region obtained from the thermomechanical analysis (Figure 10) were used for the K_I calculation. The integrity parameter, K_I, was evaluated based on the linear elastic fracture mechanics (LEFM) approach. The submodels incorporated all the boundary conditions of the RPV global model, shown in Figure 6(b), by interpolating the temporal displacements obtained from the global model as mechanical boundary conditions on the boundaries of the submodel during the simulation process. The stress intensity factor (K_1) was estimated as a function of the thermomechanical stress distribution, the assumed surface crack geometry, and the orientation using the principle of

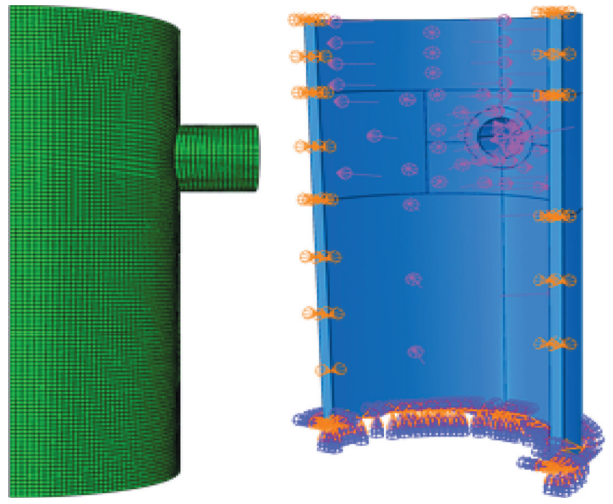

Figure 6: (a) Finite element mesh model of the RPV. (b) RPV model with applied AOO PTS loads and boundary conditions.

superposition. The K_I values were estimated at the deepest crack point using both M-integral and XFEM approaches implemented in Abaqus-FRANC3D co-simulation and Abaqus software, respectively. The surface crack geometry shown in Figure 7(b) was used for the XFEM K_I modeling process. The FE mesh surrounding the crack geometry in the submodel (Figures 8 and 9) was finely meshed so as to obtain accurate K_I and also to alleviate oscillations associated with it using the XFEM method. The mathematical computation and

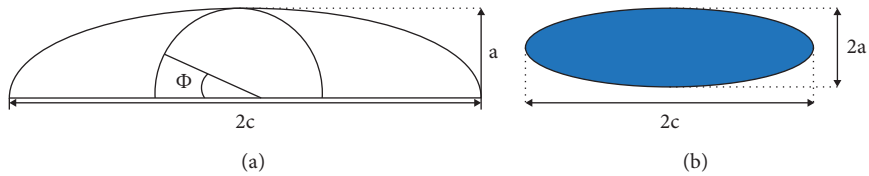

Figure 7: (a) Crack geometry details. (b) Geometric definition of surface cracks (a = crack depth; c = crack length) used in XFEM fracture analysis.

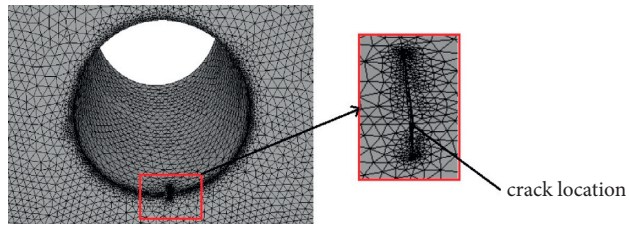

Figure 8: RPV submodel with postulated crack in FRANC3D.

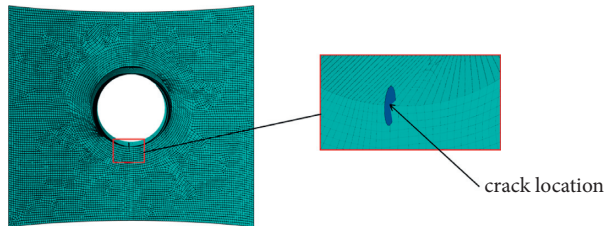

Figure 9: RPV submodel with postulated crack in Abaqus.

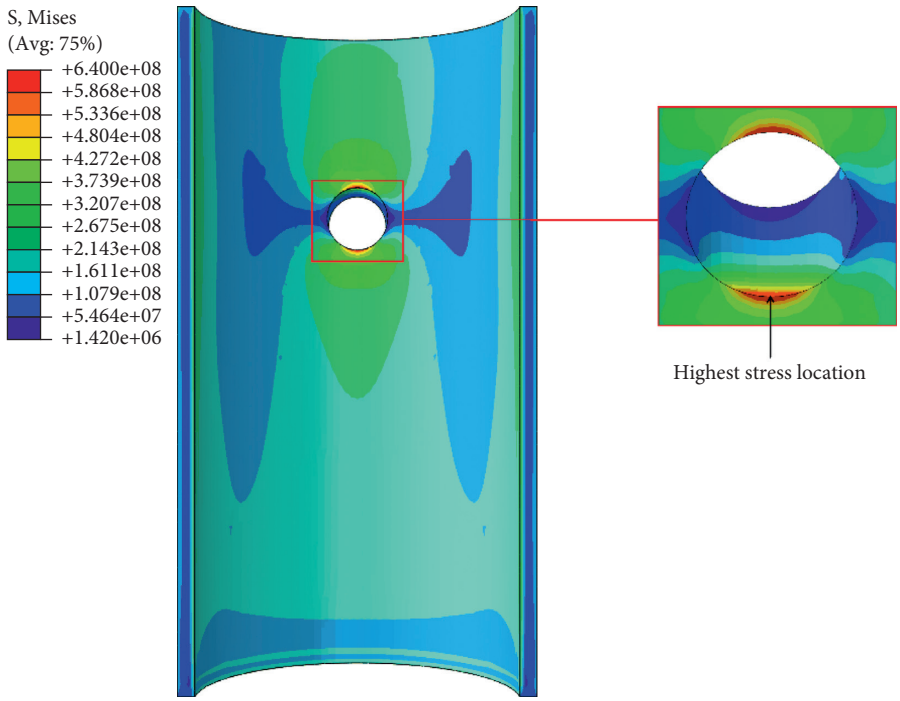

Figure 10: Maximal stress location at the inlet nozzle-inner vessel wall intersection of the RPV model.

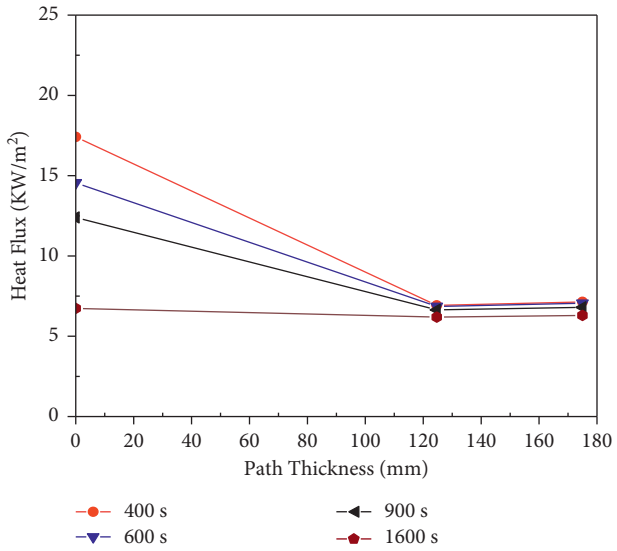

Figure 11: Heat flux distribution through the inlet nozzle-inner RPV wall intersection (path) thickness at different times.

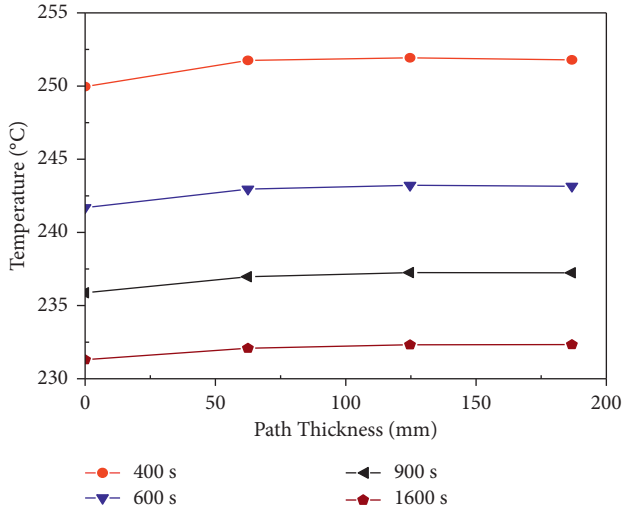

Figure 12: Temperature distribution through the inlet nozzle-inner RPV wall intersection (path) thickness at different times.

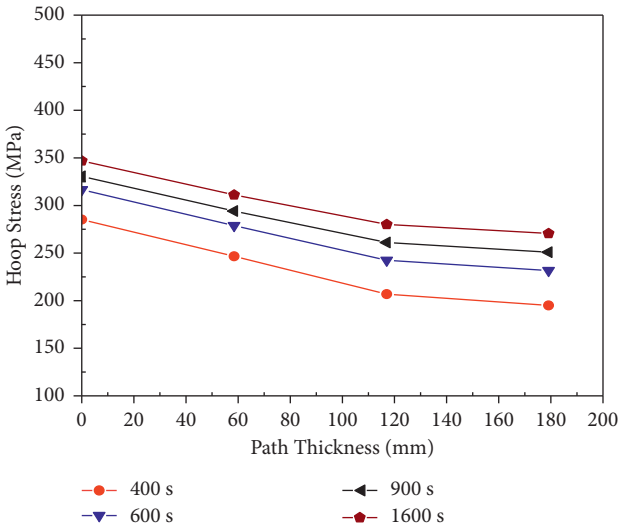

Figure 13: Hoop stress distribution through inlet nozzle-inner RPV wall intersection (path) thickness at different times.

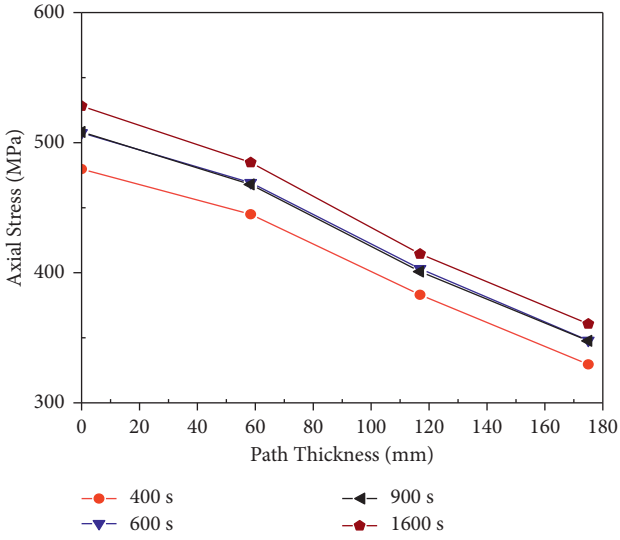

Figure 14: Axial stress distribution through inlet nozzle-inner RPV wall intersection (path) thickness at different times.

application of the M-integral energy method in computing K_I are comprehensively discussed in [36]. Also, details on the application of the XFEM method can be found in [37, 38].

4. Results and Discussion

4.1. Sequential Thermomechanical Coupling Analysis. The sequential thermomechanical analysis using the FE models described in Section 3.4 was performed in Abaqus code following the multistep procedure shown in Figure 4. The thermal loads were determined separately and then coupled with the pressure loads to compute the thermomechanical stresses. This sequential coupling analysis was to determine among others the location of the highest stress from the numerical simulation results. Figure 10 shows the von Mises stress observed at 1600 s during the AOO event. The inlet nozzle and inner RPV wall intersection (depicted in Figure 10) experienced the maximal stress concentration. The high stress was due to the complex temperature field in that joint area. Therefore, a crack-like defect was most likely to be initiated by a PTS loading at that location. The heat flux, temperature, and hoop and axial stress profiles through the thickness of inlet nozzle-inner RPV wall intersection (path), starting from the highest stress location, at different transient time periods are shown in Figures 11–14. Figures 15 and 16 also show the evolution of the temperature, hoop, and axial stresses extracted from the maximal stress element of interest in the FE model for the duration of the AOO event.

The heat flux decrease, observed through the measured thickness, was due to the steady decrease of the temperature

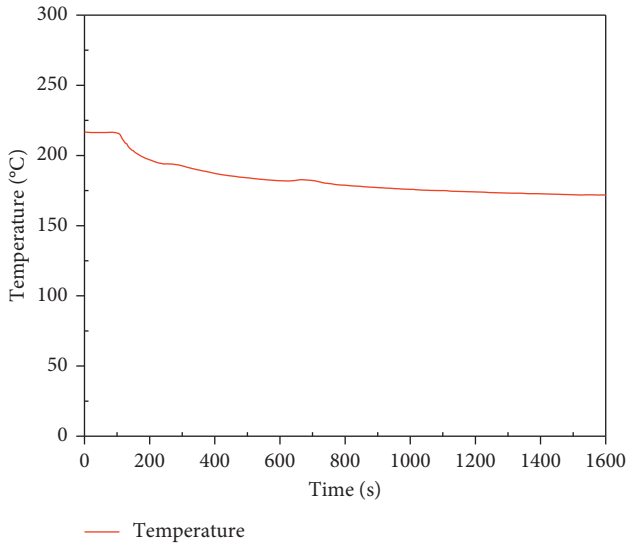

Figure 15: Temperature distribution at the maximal stress location in the RPV model during the AOO transient.

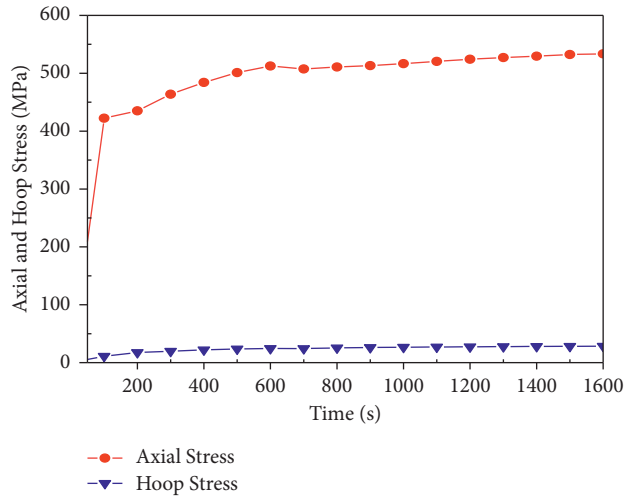

Figure 16: Axial and hoop stress distribution at the maximal stress location in the RPV model during the AOO transient.

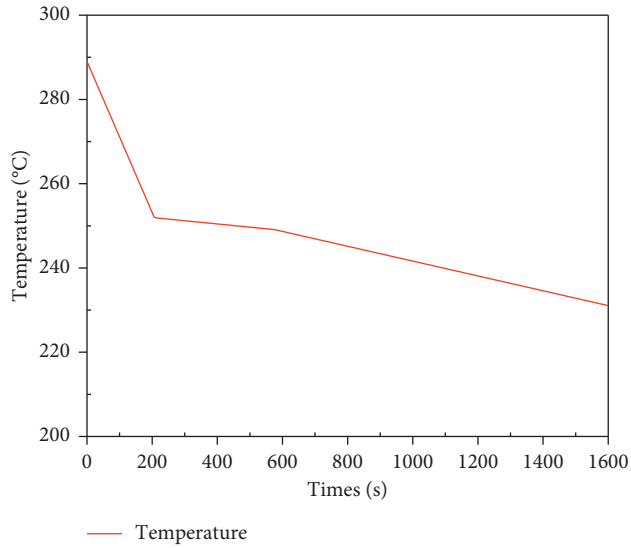

Figure 17: Temperature evolution at the deepest crack tip during the AOO transient.

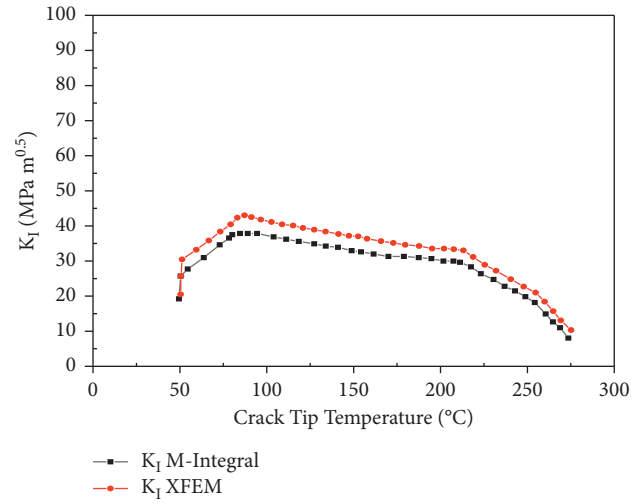

Figure 18: Comparison between M-integral and XFEM K_I estimations.

gradient and thermal conductivity. Also, the temperature gradient observed in the course of transient time decreased steadily from the inlet nozzle-inner wall RPV intersection to the outer part of the RPV model. The temperature drop was because of the sudden cooling and RPV's large thermal capacity. Furthermore, the temperature varied in the range of 60°C to 250°C through the measured thickness. This variation was due to the relatively high velocity of the cooling water injected by the actuation of HPSI pumps. Also, temperature readings in this range during this AOO transient are rated as very high in the nuclear power field. The hoop and axial stress distributions also decreased from the same maximal location to compressive stress on the outer part of the RPV wall. The hoop stress (Figure 16) exhibited a steady change throughout the transient time. Similarly, the axial stress increased steeply before remaining relatively stable from 100 s till the end of the AOO event. This phenomenon was largely due to the combined action of the thermal and internal pressure variations during the transient event.

4.2. Fracture Mechanics Analysis. The integrity parameter, K_I, was evaluated using a linear elastic fracture mechanics 3D-FE submodel with loadings obtained from the previous sequential thermomechanical coupling analysis (Section4.1). The mesh size and type of each submodel (Figures 8 and 9) were sensitively determined to ensure computational efficiency and accuracy of the stress intensity factors, K_I. Also, the K_I simulation followed the multistep coupling procedure shown in Figure 4. A semielliptical surface crack with a depth of

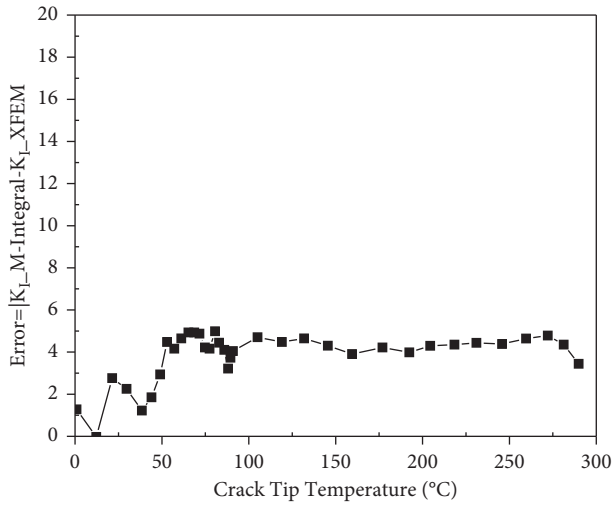

Figure 19: Error between the M-integral and XFEM K_I solutions.

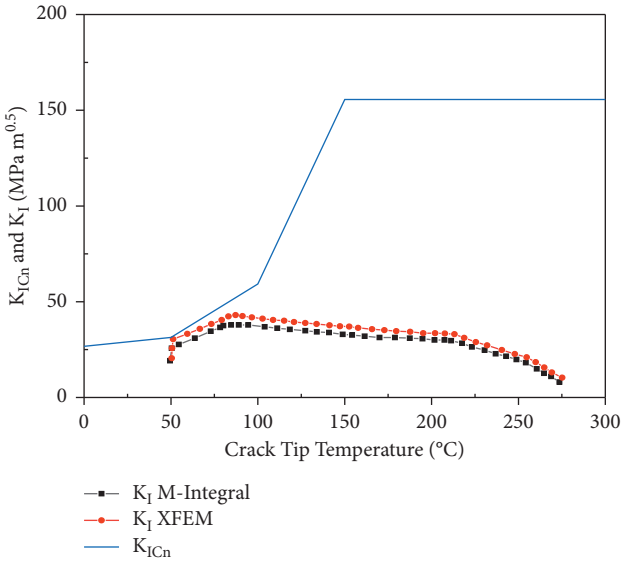

Figure 20: Comparison of K_I with K_{IC} at different crack tip temperatures.

$a = 42$ mm and an aspect ratio of $(2c/a) = 6$ was assumed for the analysis. The surface crack was inserted at the highest stress location in the RPV submodels obtained from the preceding thermomechanical analysis. The FE submodels shown in Figures 8 and 9 capture the maximal stress concentration area from the RPV global model (Figure 10) and the postulated crack orientation. In addition, the thermomechanical loads and boundary conditions applied to the FE submodels were imposed from the 3D FE model shown in Figure 6(b). The K_I values at the deepest tip of the crack were then computed using the M-integral approach coupled within the proposed sequential Abaqus-FRANC3D simulation method. To verify the K_I values obtained from the proposed method, the conventional XFEM method was also applied to compute K_I. To accurately estimate the ASME vessel material's fracture toughness, K_{IC}, the random parameters of RPV's steel shown in Table 2, were used to calculate RT_{NDT} (equation (8)). Figure 4 represents the comparison of the ASME curves generated based on RT_{NDT} values inputted in equations (9) and (10). Figure 17 shows the temperature evolution at the deepest point of the surface crack during the AOO transient. It was observed that the crack tip temperature decreased steeply for the first 200 s before remaining relatively stable through the transient time of 1600 s. The slow rate of temperature change was due to the higher heat capacity of the RPV material compared with the overcooling water.

The comparison of K_I values along the postulated crack front and crack tip temperature calculated using M-integral and XFEM methods is presented in Figure 18, and the absolute error between the K_1 estimation of both methods is shown in Figure 19. The results presented in Figures 18 and 19 show that both methods are in good agreement irrespective of the varied assumptions and numerical methods. Also, the small K_1 values observed at the deepest crack tip was due to low compressive stresses. From the comparison of K_I and K_{IC} shown in Figure 20, the maximum K_I of 43.01 $MPam^{0.5}$ was less than the upper bound fracture toughness of the vessel, K_{ICn}. In summary, the semielliptical surface crack configuration investigation results show that although the pressurized thermal shock induced by inadvertent operation of the safety injection system may not pose an immediate safety risk to the structural integrity of the RPV, it may accelerate the damage of a highly embrittled RPV with time.

5. Conclusion

One of the most frequently anticipated operational transients in a pressurized water reactor is the inadvertent operation of the safety injection systems. This transient event can induce significant pressurized thermal shocks in the reactor pressure vessel; hence, it is vital to estimate the structural mechanical changes associated with such cyclic loadings. In this paper, a sequential Abaqus-FRANC3D simulation approach was followed in the determination of the potential structural integrity risk an inadvertent operation of SIS may pose to an ageing PWR RPV. The key conclusions from the study are summarized as follows:

(1) The applied sequential Abaqus-FRANC3D simulation method efficiently reduced the computational cost in the evaluation of the AOO PTS-induced stress intensity factors. This was due to the simplified LEFM submodeling technique and FE mesh type adopted in the simulation process.

(2) The integrity parameter, K_I, calculated with M-integral and XFEM methods at the deepest crack tip was in good agreement with absolute errors of less than 5. Therefore, the K_I value obtained by the proposed sequential Abaqus-FRANC3D approach has a high accuracy and meets the precision criterion in structural engineering calculation.

(3) The K_I obtained from the AOO transient and assumed surface crack configuration investigated compared to K_{IC} shows that the effect of the SIS-

induced PTS may not pose an immediate integrity risk to the RPV, but it can cumulatively accelerate ageing mechanisms such as fatigue in the reactor pressure vessel.

This study is useful for both operators and regulators, for decision-making in reactor safety margin, ageing management, and service life extension. This work also serves as a foundation for our future study on the effect of AOO PTS loads on RPV cladding material, crack growth analysis, and fatigue life prediction.

Data Availability

Data are available from the corresponding author upon request.

Conflicts of Interest

The authors declare that they have no conflicts of interest.

Acknowledgments

This work was supported by the National Natural Science Foundation of China (Grant no. 51379046); Natural Science Foundation of Heilongjiang Province (Grant no. E2017023); and the International Atomic Energy Agency (FS-INT-1801254).

References

[1] B. Tomkins and M. F. Hamza, "Structural integrity issues in the nuclear industry," *Reference Module in Materials Science and Materials Engineering*, Elsevier Inc., Amsterdam, Netherlands, 2017.

[2] P. Trampus, "Pressurized Thermal Shock analysis of the reactor pressure vessel," *Procedia Structural Integrity*, vol. 13, pp. 2083–2088, 2018.

[3] K. Thamaraiselvi and S. Vishnuvardhan, "Fracture studies on reactor pressure vessel subjected to pressurised thermal shock: a review," *Nuclear Engineering and Design*, vol. 360, Article ID 110471, 2020.

[4] S. Miranda, "Anticipated operational occurrences that could develop into serious accidents," *Journal of Nuclear Engineering and Radiation Science*, vol. 4, no. 2, pp. 1–14, 2018.

[5] USNRC, *NRC Regulatory Issue Summary 2005-29 Anticipated Transient that Could Develop into More Serious Event*, Office of Nuclear reactor regulation, Washington, DC, USA, 2005.

[6] R. Mukin, I. Clifford, H. Ferroukhi, and M. Niffenegger, "Pressurized thermal shock (Pts) transient scenarios screening analysis with trace," *Proceedings of the 26th International Conference on Nuclear Engineering*, vol. 6a, 2018.

[7] M. Chen, F. Lu, R. Wang, and A. Ren, "Structural integrity assessment of the reactor pressure vessel under the pressurized thermal shock loading," *Nuclear Engineering and Design*, vol. 272, pp. 84–91, 2014.

[8] M. J. Jhung, S. H. Kim, Y. H. Choi et al., "Structural integrity assessment of reactor pressure vessels during pressurized thermal shock," *Journal of Mechanical Science and Technology*, vol. 22, no. 8, pp. 1451–1459, 2009.

[9] U. T. Murtaza and M. Javed Hyder, "Fracture analysis of the set-in nozzle of a PWR reactor pressure vessel-Part 1: determination of critical crack," *Engineering Fracture Mechanics*, vol. 192, pp. 343–361, 2018.

[10] S.-P. Zhu, Y.-Z. Hao, and D. Liao, "Probabilistic modeling and simulation of multiple surface crack propagation and coalescence," *Applied Mathematical Modelling*, vol. 78, pp. 383–398, 2020.

[11] X.-P. Niu, R.-Z. Wang, D. Liao, S.-P. Zhu, X.-C. Zhang, and B. Keshtegar, "Probabilistic modeling of uncertainties in fatigue reliability analysis of turbine bladed disks," *International Journal of Fatigue*, vol. 142, Article ID 105912, 2021.

[12] Y. He and T. Isozaki, "Fracture mechanics analysis and evaluation for the RPV of the Chinese Qinshan 300 MW NPP under PTS," *Nuclear Engineering and Design*, vol. 201, no. 2-3, pp. 121–137, 2000.

[13] NEA/IAEA, *Nuclear Power Plant Operating Experiences from the*, IAEA/NEA Incident Reporting System 2015-2017, International Atomic Energy Agency, Vienna, Austria, 2020.

[14] NEA/IAEA, *Nuclear Power Plant Operating Experience from the IAEA/NEA International Reporting System for Operating Experience 2005–2008*, International Atomic Energy Agency, Vienna Austria, 2010.

[15] IAEA, *Pressurized Thermal Shock in Nuclear Power Plants: Good Practices for Assessment*, International Atomic Energy Agency, Vienna, Austria, 2010.

[16] V. F. González-Albuixech, G. Qian, M. Sharabi, M. Niffenegger, B. Niceno, and N. Lafferty, "Integrity analysis of a reactor pressure vessel subjected to a realistic pressurized thermal shock considering the cooling plume and constraint effects," *Engineering Fracture Mechanics*, vol. 162, pp. 201–217, 2016.

[17] W. L. Server and R. K. Nanstad, "Integrity and embrittlement management of reactor pressure vessels (RPVs) in light-water reactors," in *Irradiation Embrittlement of Reactor Pressure Vessels (RPVs) in Nuclear Power Plants*, N. Soneda, Ed., Woodhead Publishing, Sawston, UK, 2015.

[18] AREVA, *U.S. EPR Final Safety Analysis Report*, USNRC, Rockville, ML, USA, 2013.

[19] M. Wang, Q. Zuo, H. Yu, W. Tian, G. H. Su, and S. Qiu, "Multiscale thermal hydraulic study under the inadvertent safety injection system operation scenario of typical pressurized water reactor," *Science and Technology of Nuclear Installations*, vol. 2017, Article ID 2960412, 15 pages, 2017.

[20] M. Niffenegger and K. Reichlin, "The proper use of thermal expansion coefficients in finite element calculations," *Nuclear Engineering and Design*, vol. 243, pp. 356–359, 2012.

[21] M. F. Yu, Y. J. Chao, and Z. Luo, "An assessment of mechanical properties of A508-3 steel used in Chinese nuclear reactor pressure vessels," *J Press Vess-T Asme*, vol. 137, no. 3, 2015.

[22] USNRC, *Fracture Toughness Requirements for Protection against Pressurized Thermal Shock Events*, USNRC, Rockville, ML, USA, 2012.

[23] U.S.N.R. Commission, "Radiation embrittlement of reactor vessel materials," in *Regulatory Guide*U.S.N.R.C. Office of Nuclear Regulatory Research, Rockville, ML, USA, 1988.

[24] USNRC, "Radiation embrittlement of reactor vessel materials," in *Regulatory Guide 1*USNRC, Rockville, ML, USA, 1988.

[25] X. Sun, G. Chai, and Y. Bao, "Elastic and elastoplastic fracture analysis of a reactor pressure vessel under pressurized thermal shock loading," *European Journal of Mechanics-A: Solids*, vol. 66, pp. 69–78, 2017.

[26] IAEA, *Nuclear Power Plant Operating Experiences from the*, IAEA/NEA Incident Reporting System 1999–2002, International Atomic Energy Agency, Vienna, Austria, 2003.
[27] J. P. Holman, *Heat Transfer*, McGraw-Hill Companies, Inc, New York, NY, USA, Tenth edition, 2010.
[28] H. Schlichting and K. Gersten, *Boundary-Layer Theory*, Springer-Verlag, Berlin, Heidelberg, Ninth edition, 2017.
[29] M. Faheem, N. Ramzan, and S. Naveed, "STEAMEST: a software tool for estimation of physical properties of water and steam," *Journal of Software*, vol. 4, no. 3, pp. 226–231, 2009.
[30] W. Wagner and A. Kruse, *Properties of Water and Steam/ Zustandsgrößen von Wasser und Wasserdampf*, Springer-Verlag, Berlin, Heidelberg, 1998.
[31] L. J. Young, "A fracture mechanics analysis of the PWR nuclear power plant reactor pressure vessel beltline weld," *Journal of Nuclear Materials*, vol. 288, no. 2-3, pp. 197–201, 2001.
[32] Altair, *Altair Hyper Mesh*, Altair Engineering Inc, Troy, MICH, USA, 2014.
[33] J. Mutava, M. Muvengei, K. Njoroge, and J. Kihiu, "Fracture mechanics approach to pressure vessel failures: a review," in *Proceedings of the Sustainable Research and Innovation (SRI) Conference*, Nairobi, Kenya, May 2015.
[34] IAEA, *Guidelines on Pressurized Thermal Shock Analysis for WWER Nuclear Power Plants*, International Atomic Energy Agency, Vienna, 2006.
[35] U. T. Murtaza, *Optimization and Fracture Mechanics Analysis of the Set-in Nozzle of a PWR Reactor Pressure Vessel*, Department of Mechanical Engineering, Pakistan Institute of Engineering and Applied Sciences Nilore, Islamabad, Pakistan, 2016.
[36] P. A. Wawrzynek and B. J. Carter, *The M-Integral for Computing Stress Intensity Factors in Generally Anisotropic Materials*, pp. 1–81, National Aeronautics and Space Administration, Washington, DC, USA, 2005.
[37] V. F. González-Albuixech, G. Qian, and M. Niffenegger, "Integrity analysis of reactor pressure vessels subjected to pressurized thermal shocks by XFEM," *Nuclear Engineering and Design*, vol. 275, pp. 336–343, 2014.
[38] V. F. González-Albuixech, G. Qian, M. Sharabi, M. Niffenegger, B. Niceno, and N. Lafferty, "Comparison of PTS analyses of RPVs based on 3D-CFD and RELAP5," *Nuclear Engineering and Design*, vol. 291, pp. 168–178, 2015.